

Current driven domain wall dynamics in ferrimagnetic strips explained by means of a two interacting sublattices model

Eduardo Martínez,¹ Víctor Raposo,¹ and Óscar Alejos²

¹⁾*Dpto. Física Aplicada, Universidad de Salamanca, 37008 Salamanca, Spain*

²⁾*Dpto. Electricidad y Electrónica. Universidad de Valladolid. 47011 Valladolid, Spain^{a)}*

(Dated: 17 May 2022)

The current-driven domain wall dynamics along ferrimagnetic systems are here theoretically analyzed as a function of the temperature by means of micromagnetic simulations and a one dimensional model. Contrarily to conventional effective approaches, our model takes into account the two coupled ferromagnetic sublattices forming the ferrimagnetic system. Although the model is suitable for systems with asymmetric exchange interaction and spin-orbit coupling effects due to adjacent heavy metal layers, we here focus our attention on the case of single-layer ferrimagnetic strips where domain walls adopt achiral Bloch configurations at rest. Such domain walls can be driven by either out-of-plane fields or spin transfer torques upon bulk current injection. Our results indicate that the domain wall velocity is optimized at the angular compensation temperature for both field-driven and current-driven cases. Our advanced models allow us to infer that the precession of the internal domain wall moments is suppressed at such compensation temperature, and they will be useful to interpret state-of-the art experiments on these systems.

I. INTRODUCTION

The development of racetrack memories is attracting much interest in the recent times.¹ Many efforts have been addressed in that way, particularly, the finding of optimal systems allowing fast displacement of domain walls (DWs) along them. Recent experiments show that DW velocities in the order of $1 \frac{\text{km}}{\text{s}}$ can be achieved along ferrimagnetic (FiM) strips.^{2,3} Furthermore, it has been found a linear relationship between DW velocities and the magnitude of the applied current.²⁻⁴

Based on these promising experimental results, we provide we provide a theoretical description of FiM strips based on an extended collective coordinates model (1DM)^{5,6} dealing with FiM strips. Differently from previous approaches, based on effective parameters, our model considers such systems as formed by two ferromagnetic sublattices, and coupled by means of an interlattice exchange interaction. Full micromagnetic (μM) simulations have been performed also as to back up those drawn by the collective coordinates model. Importantly, our approaches permit to infer results not achievable from effective models, and to provide insights and interesting predictions of the current-driven dynamics of DWs along FiM films.

Fig.1.(a) schematizes the local orientation of magnetic moments in the ferrimagnet. \vec{m}_i , ($i = 1, 2$) represent the orientation of the respective magnetic moments of each ferromagnetic sublattice. The magnetization of each sublattice is temperature dependent in the typical way, that is, magnetization of each sublattice vanishes at Curie temperature (T_C), with a magnetization compensation temperature T_M , as it is shown in Fig.1.(b). The temperature dependence of each magnetization can be described by the analytical functions: $M_{s,i}(T) = M_{s,i}^0 \left(1 - \frac{T}{T_C}\right)^{a_i}$, $M_{s,i}^0$ being the respective magnetizations at zero temperature,

^{a)}Electronic mail: oscar.alejos@uva.es.

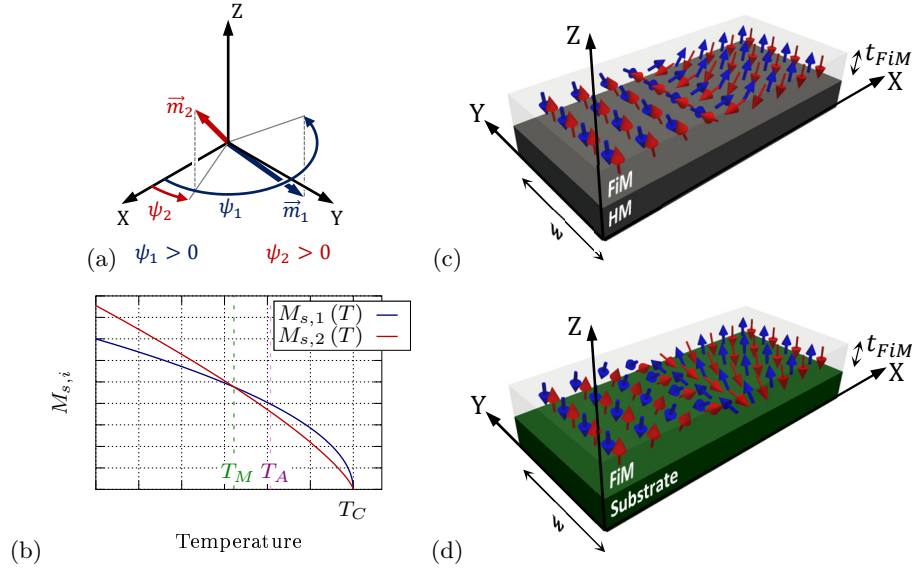


FIG. 1. Two sublattices of respective magnetizations $M_{s,1}$ and $M_{s,2}$ constitute the ferrimagnetic strip: (a) Definition of the orientation angles ψ_1 and ψ_2 of the in-plane components of the magnetization of each sublattice. Magnetizations are represented by the unit vectors \vec{m}_1 and \vec{m}_2 , (b) temperature dependence of the magnetization of each sublattice, (c) magnetic DW of Néel type amidst two domains oriented out of plane (the strip width w is here shown), and (d) magnetic DW of Bloch type amidst two domains oriented out of plane.

and a_i being some exponents depending on the sublattice components. The model can be applied to two different architectures. As a first architecture (Fig.1.(c)), a ferrimagnetic strip on top of a heavy metal (HM) can be considered. The FiM/HM interface promotes the existence of an interfacial asymmetric exchange, resulting in Néel type DWs and current driven domain wall motion (CDDWM) due to spin orbit torques. The CDDWM then involves rigid DWs. At the angular momentum compensation temperature (T_A), differing from T_M due to the distinct Landé factors g_i for each sublattice, DW magnetic moments keep aligned with the current, leading to a linear increase of DW velocities. Thus, DW velocities are maximized at T_A . This first architecture has already been adequately discussed from both the experimental³ and theoretical^{3,6} points of view, in particular, by using the model that will be here recalled⁶.

In the second architecture (Fig.1.(d)), the ferrimagnetic strip does not lie on a HM, and so interfacial asymmetric exchange vanishes. CDDWM is dominated by the spin transfer torque, and DW precessional regimes emerge, due to reduced magnetostatic interactions, resulting in DW velocities proportional to current magnitudes. Again, DW velocities have been found to maximize at T_A , when precession freezes, leading to a CDDWM characterized by rigid DWs, as it will be shown along this text.

II. TWO-SUBLATTICE MODEL OF FERRIMAGNETS

The description of the DW dynamics by means of a 1DM starts from the application of variational principles to the μM equation, i.e, the Landau-Lifshitz-Gilbert (LLG) equation.^{7,8} This procedure is then augmented to study the magnetization dynamics in FiMs by posing two coupled LLG equations. This constitutes the essence of the two-sublattice

model (TSLM), so that LLG equations for each sublattice are written as:

$$\frac{d\vec{m}_i}{dt} = -\gamma_i \vec{m}_i \times \vec{H}_{eff,i} + \alpha_i \vec{m}_i \times \frac{d\vec{m}_i}{dt} + \vec{\tau}_{STT,i} + \vec{\tau}_{SOT,i}, \quad (1)$$

where α_i represent the respective Gilbert constants of each sublattice. The effective fields $\vec{H}_{eff,i}$ comprise all interactions within the system, i.e., all intra-sublattice interactions along with an interaction term between both sublattices, that is:

$$\vec{H}_{eff,i} = \vec{H}_{ext} + \vec{H}_{dmg,i} + \vec{H}_{ani,i} + \vec{H}_{exch,i} + \vec{H}_{D,i}. \quad (2)$$

\vec{H}_{ext} , $\vec{H}_{dmg,i}$, $\vec{H}_{ani,i}$ are respectively the external field, with components (H_x, H_y, H_z) , the demagnetizing (magnetostatic) field, the anisotropy field, whose out-of-plane and in-plane components are given by the effective anisotropy constants $K_{eff,i}$ and $K_{sh,i}$, the isotropic exchange field and the asymmetric exchange field. $\vec{H}_{D,i}$ accounts for the chiral nature of some magnetic textures, being determined by some constants D_i , and $\vec{H}_{exch,i}$ can be reduced on first approach to the sum of terms:⁹

$$\vec{H}_{exch,i} = \frac{2A_i}{\mu_0 M_{s,i}} \nabla^2 \vec{m}_i + \frac{2A_{ij}}{\mu_0 M_{s,i}} \nabla^2 \vec{m}_j + \frac{B_{12}}{\mu_0 M_{s,i}} \vec{m}_j, \quad (3)$$

being $j = 1, 2$, and $j \neq i$. The first term here stands for an intra-sublattice exchange field, given by the exchange stiffness A_i . The middle term represents a sublattice exchange due to the local variations of the magnetization in the other sublattice, then slightly affecting the DW width.¹⁰ This term can be easily implemented into μ M simulation codes.⁵ However, since the 1DM takes in general the DW width as an input, such a term loses relevance in substantiating the results of the model. The latter term in Eq.(3) is an inter-sublattice interaction due to the misalignment of both sublattices, which is derived from an energy density expression in the form $\epsilon_{12} = -B_{12} \vec{m}_1 \cdot \vec{m}_2$, so that $B_{12} > 0$ (< 0) promotes the antiparallel (parallel) alignment of the sublattices. Finally, $\vec{\tau}_{STT,i}$ and $\vec{\tau}_{SOT,i}$ represent the torques due to spin polarized currents, i.e., the spin transfer torques⁷ and the spin-orbit torques⁸, respectively. The former terms consist of adiabatic interactions $\vec{\tau}_{A,i}$, defined by certain values u_i , and their non-adiabatic counterparts $\vec{\tau}_{NA,i}$, related to these by the factors β_i , so that:

$$\begin{aligned} \vec{\tau}_{STT,i} &= \vec{\tau}_{A,i} + \vec{\tau}_{NA,i} = \\ &= u_i (\vec{u}_J \cdot \nabla) \vec{m}_i - \beta_i u_i \vec{m}_i \times (\vec{u}_J \cdot \nabla) \vec{m}_i, \end{aligned} \quad (4)$$

where \vec{u}_J represents the direction of the current density. The values u_i are proportional to the electric density current J_x , flowing along the system, and are calculated as $u_i = \frac{1}{2} \frac{q_i \mu_B P}{e M_{s,i}} J_x$, with μ_B being Bohr's magneton, e is the electron charge, and P is the degree of polarization of the spin current.

The SOT includes field-like (FL) and Slonczewskii-like (SL) contributions, with respective fields $H_{FL,i}$, and $H_{SL,i}$:

$$\begin{aligned} \vec{\tau}_{SOT,i} &= \vec{\tau}_{FL,i} + \vec{\tau}_{SL,i} = \\ &= -\gamma_i H_{FL,i} \vec{m}_i \times \vec{\sigma} - \gamma_i H_{SL,i} \vec{m}_i \times (\vec{m}_i \times \vec{\sigma}), \end{aligned} \quad (5)$$

where $\vec{\sigma}$ is the unit vector along the direction of the polarization of the spin current generated by SHE in the HM, that is, $\vec{\sigma} = \vec{u}_J \times \vec{u}_z$, since \vec{u}_z defines the HM/FiM interface.^{7,11,12}

Prior to the derivation of the 1DM, the DW profile must be described in terms of the DW position q , width Δ and transition type Q . In the TSLM, the DW is considered to be composed of two transitions, one for each sublattice, which share the same q , and the same Δ (see Fig.1.(c) and (d)), but $Q_i = \pm 1$ establishes the transition type for each sublattice. $Q_i = +1$ (-1) means up-down (down-up) transition. Due to the antiferro coupling between

sublattices, it follows that $Q_1 = -Q_2$. The set of equations determining DW dynamics in the system can be deployed:⁶

$$\begin{aligned} \alpha_1 \frac{M_{s,1}}{\gamma_1} \frac{\dot{q}}{\Delta} + \alpha_2 \frac{M_{s,2}}{\gamma_2} \frac{\dot{q}}{\Delta} + \frac{M_{s,1}}{\gamma_1} Q_1 \dot{\psi}_1 + \frac{M_{s,2}}{\gamma_2} Q_2 \dot{\psi}_2 = \\ = Q_1 M_{s,1} \left[H_z - \frac{\pi}{2} H_{SL,1} \cos \psi_1 \right] + \\ + Q_2 M_{s,2} \left[H_z - \frac{\pi}{2} H_{SL,2} \cos \psi_2 \right] + \\ + \frac{M_{s,1}}{\gamma_1} \beta_1 \frac{u_1}{\Delta} + \frac{M_{s,2}}{\gamma_2} \beta_2 \frac{u_2}{\Delta}, \end{aligned} \quad (6a)$$

$$\begin{aligned} -Q_1 \frac{\dot{q}}{\Delta} + \alpha_1 \dot{\psi}_1 = -Q_1 \frac{u_1}{\Delta} - \gamma_1 \frac{H_{k,1}}{2} \sin(2\psi_1) + \\ + \gamma_1 \frac{\pi}{2} Q_1 H_{D,1} \sin \psi_1 - \gamma_1 \frac{\pi}{2} H_{FL,1} \cos \psi_1 + \\ + \gamma_1 \frac{\pi}{2} (H_y \cos \psi_1 - H_x \sin \psi_1) + \\ + \gamma_1 \frac{2B_{12}}{\mu_0 M_{s,1}} \sin(\psi_1 - \psi_2), \end{aligned} \quad (6b)$$

$$\begin{aligned} -Q_2 \frac{\dot{q}}{\Delta} + \alpha_2 \dot{\psi}_2 = -Q_2 \frac{u_2}{\Delta} - \gamma_2 \frac{H_{k,2}}{2} \sin(2\psi_2) + \\ + \gamma_2 \frac{\pi}{2} Q_2 H_{D,2} \sin \psi_2 - \gamma_2 \frac{\pi}{2} H_{FL,2} \cos \psi_2 + \\ + \gamma_2 \frac{\pi}{2} (H_y \cos \psi_2 - H_x \sin \psi_2) + \\ + \gamma_2 \frac{2B_{12}}{\mu_0 M_{s,2}} \sin(\psi_2 - \psi_1), \end{aligned} \quad (6c)$$

III. RESULTS AND DISCUSSION

When FiMs, such as GdFeCo or Mn₄N, are grown on top of certain substrates, the absence of interfacial asymmetric exchange^{2,13} results in the formation of achiral DWs. The orientation of DW internal moments at rest is then dependent on purely geometrical aspects. In particular, for thin strips sufficiently wide, magnetostatic interactions determine the formation of Bloch-type walls. Importantly, due to the low net magnetization of FiMs as compared with ferromagnets, the magnetostatic interactions are rather low. If some parallelism between ferro- and ferrimagnets is made, Walker breakdown in FiMs is then expected to occur for rather low applied fields¹⁴ or currents^{15,16} in the temperature range around T_M . Consequently, the DW dynamics for moderate fields or currents is ruled by the precession of DW magnetic moments.

The case of the field-driven DW dynamics in ferrimagnetic GdFeCo alloys can be recalled at this point. This has been the subject of recent experimental work,² where fast field-driven antiferromagnetic spin dynamics is realized in FiMs at T_A . This behavior has been found to be reproducible with the two-sublattice model here presented.

In order to carry out our simulations, a set of parameters for the two sublattices ($i = 1, 2$) have been chosen similar to those considered in previous works^{3,6}, but adapted so that to take into account the absence of interfacial asymmetric exchange and SOTs. The parameters are: $A_i = 70 \frac{\text{pJ}}{\text{m}}$, $K_{eff,i} \approx K_{u,i} = 1.4 \frac{\text{MJ}}{\text{m}^3}$, $K_{u,i}$ being the magnetic uniaxial anisotropy constant of the FiM sublattices. With these parameters, DW width is $\Delta \approx 6\text{nm}$. Besides, $\alpha_i = 0.02$, $D_i = 0 \frac{\text{mJ}}{\text{m}^2}$, $H_{SL,i} = H_{FL,i} = 0$. Due to the low net magnetization in the temperature range of interest, $K_{sh,i} \approx 0$. The antiferromagnetic coupling between the two

sublattices is accounted for by the parameter $B_{12} = -90 \frac{\text{MJ}}{\text{m}^3}$.⁹ The gyromagnetic ratios ($\gamma_i = \frac{g_i \mu_B}{\hbar}$) are different due to distinct Landé factors: $g_1 = 2.2$ and $g_2 = 2.0$.² The temperature dependence of the magnetization of each sublattice is determined by the Curie temperature $T_C = 450\text{K}$ of the FiM, and $M_{s,1}^0 = 1.4 \frac{\text{MA}}{\text{m}}$ and $M_{s,2}^0 = 1.71 \frac{\text{MA}}{\text{m}}$, with $a_1 = 0.5$ and $a_2 = 0.76$. According to these values, $T_M \approx 241.5\text{K}$, and $T_A \approx 305\text{K}$. The dimensions of the FiM strips are $w \times t_{\text{FiM}} = 512\text{nm} \times 6\text{nm}$.

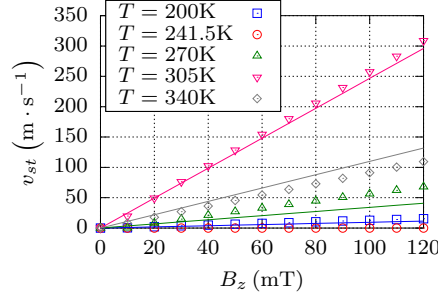


FIG. 2. Terminal velocity as a function of the out-of-plane applied field B_z at different temperatures. Dots and continuous lines correspond respectively to full μM simulations and the 1DM results.

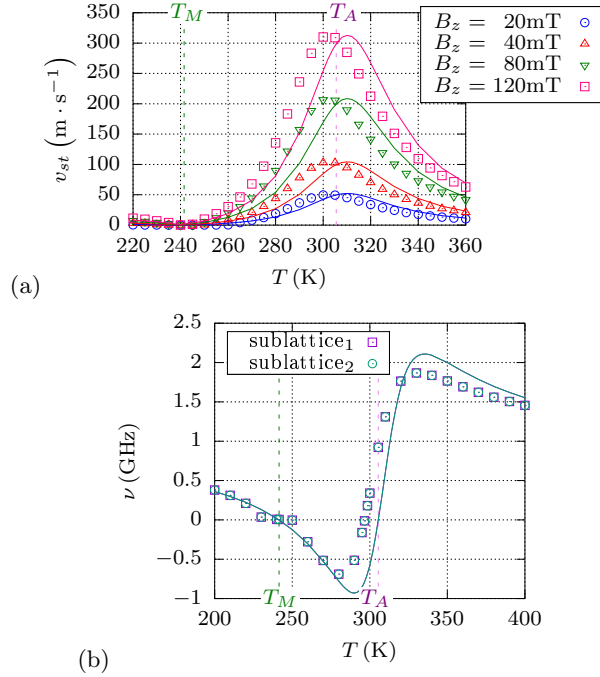


FIG. 3. (a) Terminal velocity and (b) precessional frequencies of DWs in a FiM strip with no interfacial asymmetrical exchange as a function of temperature. The out-of-plane applied field B_z is taken as a parameter in (a), whereas $B_z = 40\text{mT}$ is considered in (b). Dots and continuous lines correspond respectively to full μM simulations and the 1DM results, with a good agreement between both approaches.

Fig.2 presents the dependence of the DW terminal speed, computed as $v_{st} = \frac{q(\Delta t) - q(0)}{\Delta t}$, with $\Delta t = 2\text{ns}$, on the out-of-plane applied field B_z at different temperatures. In agreement with experiments,² v_{st} increase linearly with B_z , and the slope reaches a maximum at T_A . This fact is made clear in Fig.3.(a) where terminal velocities are represented as a function

of temperature with B_z as a parameter. In all shown cases, no dynamics occurs at T_M since the net magnetization vanishes, whereas the highest speeds are found close to T_A . The clue for this behavior can be found in DW precession, whose frequency is obtained as $\nu = \frac{\dot{\psi}_i(\Delta t)}{2\pi}$ ($i = 1, 2$), since $\dot{\psi}_1(\Delta t) \approx \dot{\psi}_2(\Delta t)$, represented as a function of temperature in Fig.3.(b). The results demonstrate that during the dynamics, magnetic moments within the DW precess except at temperatures around T_M and T_A , where precession freezes and the orientation of DW magnetic moments during the whole dynamics holds.

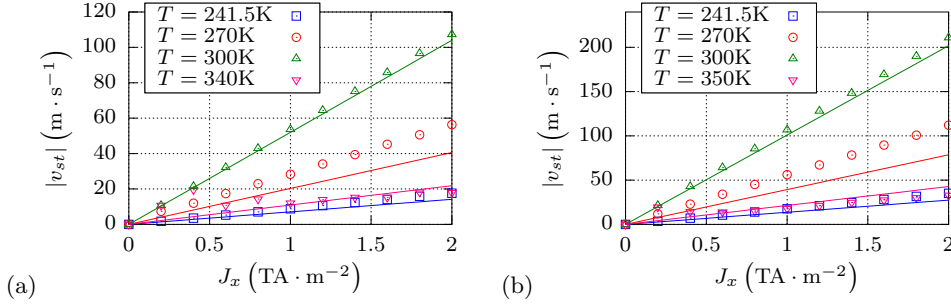


FIG. 4. Terminal velocity as a function of the electric density current J_x at different temperatures. Dots and continuous lines correspond respectively to full μM simulations and the 1DM results in the cases: (a) $\beta_i = \alpha_i$, and (b) $\beta_i = 2\alpha_i$

Previous field-driven analysis serves as a starting point to also understand the CDDWD in these systems. This dynamics is purely governed by STT because DWs move contrary to the current direction.¹³ Fig.4 presents the dependence of the absolute terminal velocities as a function of the current J_x with the temperature as a parameter. The polarization has been set to $P = 0.7$, and the non-adiabatic transfer torque parameters have been chosen as (a) $\beta_i = \alpha_i$, and (b) $\beta_i = 2\alpha_i$. Differently from the results obtained in the field-driven case, the CDDWD at T_M is no null, since the STT pushes the transitions in each sublattice in the same direction (and not in opposite directions as it occurs in the field-driven case). However, the maximum slope is again found at T_A .

The plot of the absolute terminal velocities as a function of temperature shown in Fig.5.(a) and (c) confirms that the fastest dynamics occurs again at T_A , as in the preceding case. Besides, the precessional frequencies are plotted in Fig.5.(b) and (d). It can be found again that precession freezes around T_A .

To show in more detail this behavior, Fig.6 presents the snapshots of the CDDWD at two representative temperatures, for the case $\beta_i = \alpha_i$. In order to simplify the view, the two sublattices composing the FiM are presented superposed, so one sublattice is on top of the other. The images in (a) correspond to the dynamics at $T < T_A$. In this case, the DW internal moments precess so that a turn of approximately 180° takes place within the 1ns-interval passing from the image on top to the bottom image. However, no precession takes place at $T = T_A$, as shown in (b). The different distances run by the DWs can be also compared.

Differently from the behavior of magnetic moments in pure ferromagnets, where STT compensates damping when $\beta_i = \alpha_i$, FiMs seem to present these precessing magnetic moments even in this case. Such precession would be associated with the torque due to the coupling between the two sublattices and freezes at T_A , a result that would not be in any case explainable by means of effective models.

IV. CONCLUSIONS

The aim of this work has been first to highlight the capacities of the TSLM and, particularly, the 1DM based on it to reproduce recent experimental work on DW dynamics in

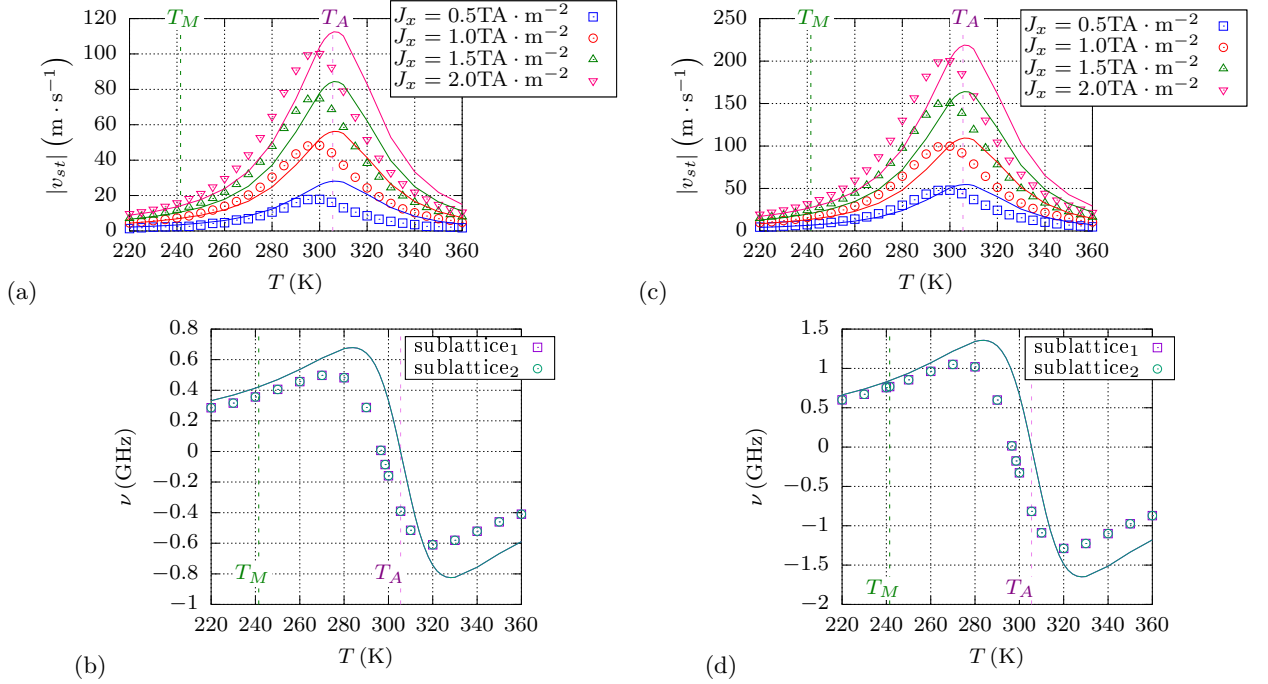


FIG. 5. Terminal velocity and precessional frequencies of DWs in a FiM strip with no interfacial asymmetrical exchange as a function of temperature with the electric density current J_x as a parameter. The cases shown are: (a) terminal velocity for $\beta_i = \alpha_i$, (b) precessional frequency for $\beta_i = \alpha_i$ (a) terminal velocity for $\beta_i = 2\alpha_i$, and (d) precessional frequency for $\beta_i = 2\alpha_i$. Dots and continuous lines correspond respectively to full μM simulations and the 1DM results. The highest velocity is reached at a temperature around T_A , when the precessional frequency vanishes.

FiMs. Differently from previous approaches, the TSLM do not require the use of effective parameters, but experimentally determined ones, which allows providing insightful details about the dynamics.

The work has been devoted to FiMs structured so that DWs adopt achiral Bloch configurations at rest, and the main conclusions of this work are as following. The DW dynamics in FiMs is characterized by DW precession, which freezes at T_A . Because of that, the DW velocity at T_A is enhanced, both for the field- and for the current-driven cases. Our results are also in good qualitative agreement with recent experimental observations: Ref.2 for the field-driven case, and Ref.13 for the current-driven one. Finally, the physical origin or the fundamental reasons behind these observations can only be achieved by adopting models which take into account the independent but antiferromagnetic coupled nature of the two sublattices forming the FiM. Therefore, our models will be useful to understand state-of-the-art experiments and also to develop and optimize future DW-based devices.

V. ACKNOWLEDGEMENT

This work was partially supported by Project No. MAT2017-87072-C4-1-P from the (Ministerio de Economía y Competitividad) Spanish Government and Project No. SA299P18 from Consejería de Educación Junta de Castilla y León.

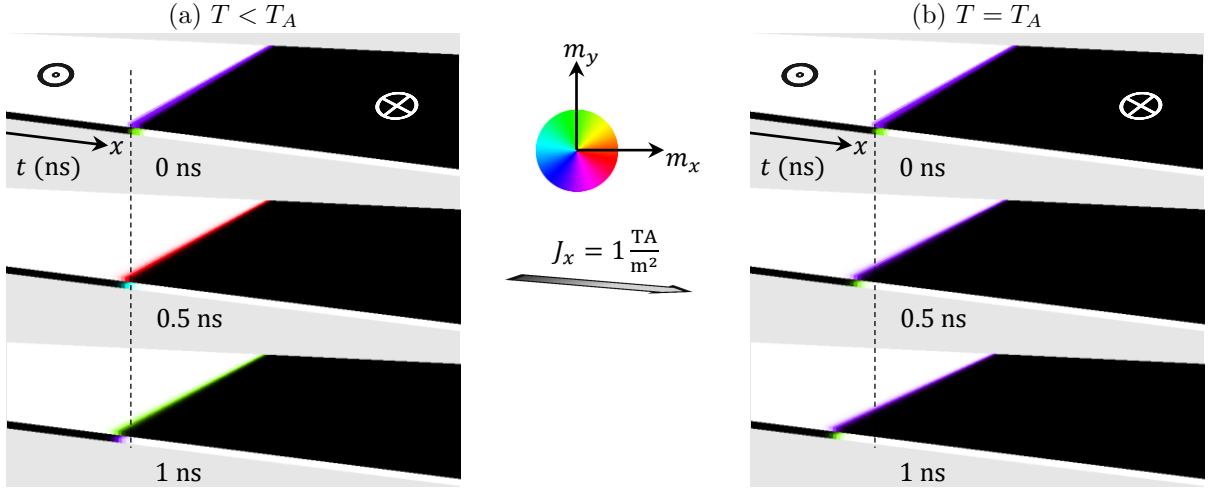


FIG. 6. Snapshots of the DW dynamics in a FiM with $\beta_i = \alpha_i$ at two different temperatures: (a) $T < T_A$, and (b) $T = T_A$. Dots and continuous lines correspond respectively to full μM simulations and the 1DM results. At T_A the magnetic moments within the DW stop precessing, and the terminal velocity reaches a maximum.

VI. BIBLIOGRAPHY

- ¹S. S. P. Parkin, M. Hayashi, and L. Thomas, “Magnetic domain wall racetrack memory,” *Science* **320**, 190 (2008).
- ²K.-J. Kim, S. K. Kim, Y. Hirata, S.-H. Oh, T. Tono, D.-H. Kim, T. Okuno, W. S. Ham, S. Kim, G. Go, Y. Tserkovnyak, A. Tsukamoto, T. Moriyama, K.-J. Lee, and T. Ono, “Fast domain wall motion in the vicinity of the angular momentum compensation temperature of ferrimagnets,” *Nature Materials* **16**, 1187–1192 (2017).
- ³L. Caretta, M. Mann, F. Büttner, K. Ueda, B. Pfau, C. M. Günther, P. Helsing, A. Churikova, C. Klose, M. Schneider, D. Engel, C. Marcus, D. Bono, K. Bagschik, S. Eisebitt, and G. S. D. Beach, “Fast current-driven domain walls and small skyrmions in a compensated ferrimagnet,” *Nature Nanotechnology* **3** (2018).
- ⁴S. A. Siddiqui, J. Han, J. T. Finley, C. A. Ross, and L. Liu, “Current-induced domain wall motion in a compensated ferrimagnet,” *Physical Review Letters* **121**, 057701 (2018).
- ⁵Ó. Alejos, V. Raposo, L. Sanchez-Tejerina, R. Tomasello, G. Finocchio, and E. Martinez, “Current-driven domain wall dynamics in ferromagnetic layers synthetically exchange-coupled by a spacer: A micromagnetic study,” *Journal of Applied Physics* **123**(1), 013901 (2018).
- ⁶E. Martínez, V. Raposo, and Ó. Alejos, “Current-driven domain wall dynamics in ferrimagnets: Micromagnetic approach and collective coordinates model,” *Journal of Magnetism and Magnetic Materials* **491**, 165545 (2019).
- ⁷P. P. J. Haazen, E. Mure, J. H. Franken, R. Lavrijsen, H. J. M. Swagten, and B. Koopmans, *Nature Materials* **12**, 299 (2013).
- ⁸S. Zhang and Z. Li, *Physical Review Letters* **93**, 1 (2004).
- ⁹C. T. Ma, X. Li, and S. J. Poon, “Micromagnetic simulation of ferrimagnetic tbfeo films with exchange coupled nanophases,” *Journal of Magnetism and Magnetic Materials* **417**, 197–202 (2016).
- ¹⁰L. Sánchez-Tejerina, V. Puliafito, P. K. Amiri, M. Carpentieri, and G. Finocchio, “Dynamics of domain walls motion driven by spin-orbit torque in antiferromagnets,” (2019), arXiv:1904.02491 [cond-mat.mes-hall].
- ¹¹K.-S. Ryu, L. Thomas, S.-H. Yang, and S. Parkin, *Nature Nanotechnology* **8**, 527–533 (2013).
- ¹²S. Emori, U. Bauer, S.-M. Ahn, E. Martínez, and G. Beach, *Nature Materials* **12**, 611–616 (2013).
- ¹³T. Gushi, M. Jovičević Klug, J. Peña García, H. Okuno, J. Vogel, J. P. Attané, T. Suemasu, S. Pizzini, and L. Vila, “ mn_4n ferrimagnetic thin films for sustainable spintronics,” (2019), arXiv:1901.06868 [cond-mat.mtrl-sci].
- ¹⁴A. Mougin, M. Cormier, J. P. Adam, P. J. Metaxas, and J. Ferré, “Domain wall mobility, stability and walker breakdown in magnetic nanowires,” *Europhysics Letters* **5**, 57007 (2007).
- ¹⁵A. Thiaville, Y. Nakatani, J. Miltat, and N. Vernier, *Journal of Applied Physics* **95**(11), 7049 (2004).
- ¹⁶A. Thiaville, Y. Nakatani, J. Miltat, and Y. Suzuki, *Europhysics Letters* **69**, 990 (2005).